crystals

MDPI

Communication

Crystal Plasticity Simulation of the Microstructural Effect in Powder Metallurgy Superalloys under Dwell Fatigue Loading

Zebang Zheng [1,2,*,†] and Zichao Peng [3,*,†]

[1] Research & Development Institute of Northwestern Polytechnical University in Shenzhen, Northwestern Polytechnical University, Shenzhen 518057, China
[2] State Key Laboratory of Solidification Processing, Shaanxi Key Laboratory of High-Performance Precision Forming Technology and Equipment, School of Materials Science and Engineering, Northwestern Polytechnical University, Xi'an 710072, China
[3] Science and Technology on Advanced High Temperature Structural Materials Laboratory, Beijing Institute of Aeronautical Materials, AECC, Beijing 100095, China
* Correspondence: zebang.zheng@nwpu.edu.cn (Z.Z.); pengzichaonbanba7@hotmail.com (Z.P.)
† These authors contributed equally to this work.

Abstract: The microstructural effect, including γ′ precipitate morphology and twin grains, of dwell fatigue behavior in a powder metallurgy nickel-based superalloy, was studied using crystal plasticity modeling. Strain rate and dwell sensitivities of 923 K were quantitatively investigated. The strain accumulations, under normal and dwell fatigue loading, showed γ′ precipitate size-dependence. Strong load shedding can be observed between parent and twin grains, which was attributed to local plastic heterogeneity. Local stress and strain evolution are both faster than the macroscopic values, which threatens the safety of engine components.

Keywords: load shedding; microstructure; size effect; γ′ precipitate; dwell fatigue

check for updates

Citation: Zheng, Z.; Peng, Z. Crystal Plasticity Simulation of the Microstructural Effect in Powder Metallurgy Superalloys under Dwell Fatigue Loading. *Crystals* **2022**, *12*, 269. https://doi.org/10.3390/cryst12020269

Academic Editors: Huamiao Wang, Guowei Zhou and Indrajit Charit

Received: 18 January 2022
Accepted: 16 February 2022
Published: 16 February 2022

Publisher's Note: MDPI stays neutral with regard to jurisdictional claims in published maps and institutional affiliations.

Copyright: © 2022 by the authors. Licensee MDPI, Basel, Switzerland. This article is an open access article distributed under the terms and conditions of the Creative Commons Attribution (CC BY) license (https://creativecommons.org/licenses/by/4.0/).

1. Introduction

Powder metallurgy (PM) nickel-based superalloys have been widely used in aero-engine disks, owing to their excellent creep and fatigue resistance at high temperatures [1–3]. The mechanical performance of these alloys is fundamentally related to the morphology of the solution strengthening precipitates. The FGH96 superalloy, for example, demonstrated different creep behaviors and fracture mechanisms resulting from differing γ′ precipitate sizes [4]. Precipitate distribution within the alloy can be controlled by designing an appropriate solution treatment route [5] to achieve better macroscopic properties.

The stress-bearing components in the engines are generally subjected to low cycle dwell fatigue (LCDF) loading conditions. This results in a serious lifetime reduction of the components compared to normal fatigue and pure creep. Dwell sensitivity was initially investigated for titanium alloys [6–10], but not for superalloys. The explanation for early crack formation under dwell fatigue is that stress redistribution, namely load shedding amongst crystallographic soft–hard grain combinations occurring during the dwell period, [11] arises from the remarkable anisotropy observed in the hexagonal close-packed structure. A significant amount of plasticity accumulated in the soft grain by the manifestations of strain rate sensitivity (SRS) leads to stress concentrations in the neighboring hard grain and, eventually, causes facet crack formation. Nickel-based superalloys also experience a strong strain rate and dwell sensitivity, similar to titanium alloys, although the underlying failure mechanism may differ. On the one hand, the crystal structure in the superalloys is mainly face-centered cubic, hence, the crystallographic anisotropy is weaker than titanium. On the other hand, there is no evidence indicating that facets can be formed in superalloys under dwell fatigue.

Nevertheless, the rate dependence of plasticity has been demonstrably affected by the microstructures in both alloys [12–14]. In particular, the creep behavior of PM nickel-based superalloys has shown strong correlations with the γ′ precipitate morphology [4]. The different creep rates, with respect to the γ′ precipitate's size, can be documented using the crystal plasticity (CP) model [15]. However, the mechanistic effect of the γ′ precipitate on dwell fatigue responses, especially at critical locations, e.g., twin boundaries, remains elusive.

Investigations into the microstructural effects of plastic deformation, especially plasticity localization near twin boundaries in nickel-based superalloys, have been launched in recent years. Stinville and co-authors [16,17] characterized the local strain and strain heterogeneities under fatigue loadings by employing the high-resolution digital image correlation (DIC) technique. They observed that the strain concentration at grain boundaries, induced due to the resistance to slip transmission, can be up to eight times higher than the nominal strain. More recently, Latypov et al. [18] found that the extent and intensity of strain localizations are governed by grain shape and orientation using an integrated microstructure-based CP modeling and DIC characterization method. Zhang et al. [19] focused on crystallography and elastic anisotropy at twin boundaries in nickel superalloy under fatigue conditions. The results suggested that twin boundaries may lead to strongly elevated locally stored energy densities, which is argued to drive fatigue crack nucleation. The aforementioned evidence indicates that plasticity localizations near twin boundaries are crucial prerequisites for fatigue responses in nickel-based superalloys and, therefore, these microstructural features need to be explicitly represented in order to capture this phenomenon.

This study focuses on the fatigue responses of PM nickel-based superalloys with different precipitate sizes by employing a microstructure-based crystal plasticity modeling approach in which the grain morphology is explicitly represented, aiming to shed light on the mechanistic basis of the dwell fatigue failure.

2. Materials and Crystal Plasticity Finite Element Framework

The material of interest here is an FGH96 alloy manufactured using the powder metallurgy technique. The specimens were solution-treated following four different cooling rates in the air to generate four different γ′ precipitate sizes, i.e., 46.3 nm, 49.7 nm, 68.7 nm, and 88.8 nm. The volume fractions of the γ′ precipitates are 49.7%, 49.6%, 48.8%, and 45.4%, respectively. For convenience, the corresponding specimens are named in conjunction with the γ′ precipitates' sizes as S1, S2, S3, and S4, respectively. The detailed heat-treatment routes can be found in ref. [4]. To characterize the grain morphology and γ′ precipitate distributions, electron back-scattered diffraction (EBSD) and a high-resolution scanning electron microscope (HR-SEM) were used upon the four specimens. Additionally, high-temperature stress-relaxation tests were conducted using specimens with different γ′ precipitates to evaluate their strain rate sensitivities. The loading temperature for both the experiment and simulation in this study was 650 °C. Cylindrical dog-bone-shaped specimens with a gauge length of 32 mm and a diameter of 5.5 mm were machined. The material was uniaxially stretched, from a strain-free status to a constant engineering strain rate of 2.5×10^{-4} s^{-1}, up to 4%, followed by a strain-hold period at the maximum value for 540 s where stress relaxation can be observed due to creep behaviors. The stress-strain curves and microstructure characterizations are summarized in Figure 1.

The crystal plasticity finite element modeling utilized in this work is a rate-dependent framework based on a realistic microstructure. Since there is no significant difference at the grain level, including grain shapes and textures, for these specimens, as shown in Figure 1, one of the EBSD maps was used to construct the geometry of the model. All the critical microstructural features, including twin grains and crystal orientations, were replicated in the morphology model, as shown in the inset of Figure 1. The model size is 75 μm × 75 μm × 5 μm, which consists of 139 grains and was meshed by 27,420 C3D20R

elements. The grains were extruded along the thickness direction and a plane stress condition was applied.

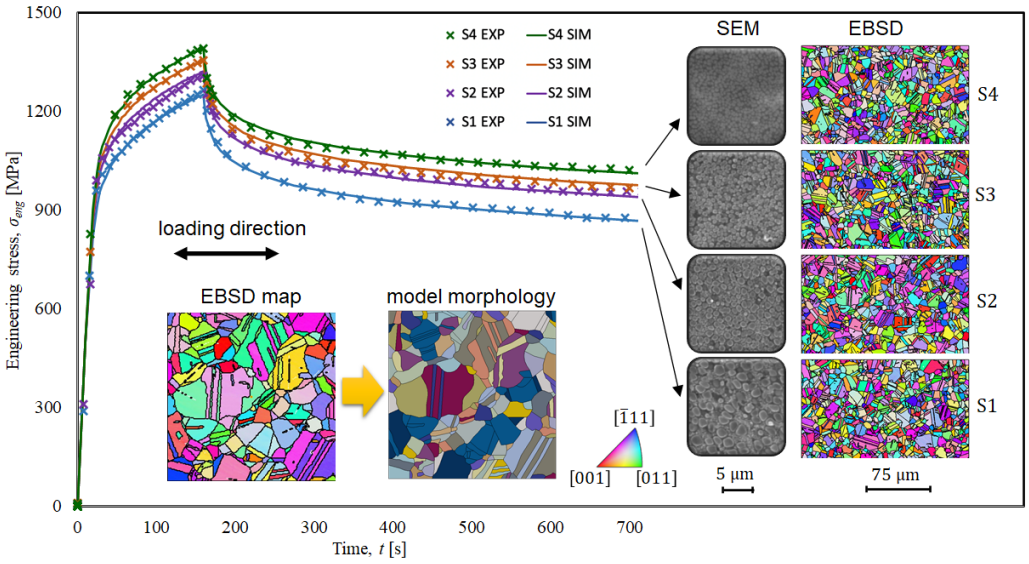


Figure 1. Calibrations of the stress-relaxation results for the superalloys with four different γ' precipitate sizes using crystal plasticity based on realistic microstructures.

The slip rule of the crystal plasticity model was developed based on the dislocation thermally activated escaping from pinned obstacles by considering both forward and backward jumps [20]. The resolved crystallographic plastic slip rates on each slip plane (i) is given by

$$\dot{\gamma}^{(i)} = \rho_m b^2 \nu_D \exp\left(-\frac{\Delta F}{kT}\right) \sinh\left(\frac{\left(\tau^{(i)} - \tau_c^{(i)}\right)\Delta V}{kT}\right) \tag{1}$$

where $\rho_m = 10\ \mu\text{m}^{-2}$ is the mobile dislocation density, $b = 0.254$ nm is the Burgers vector, $\nu_D = 10^{11}\ \text{s}^{-1}$ is the Debye frequency, $k = 1.381 \times 10^{-23}$ J/K is the Boltzmann constant, $\tau^{(i)}$ and $\tau_c^{(i)}$ are the resolved and critical resolved shear stress (CRSS) on slip system i, respectively, ΔF is the activation energy, and ΔV is the activation volume. The considered temperature is $T = 923$ K, which is the typical in-service temperature of FGH96 turbine disks. There are 12 available slip systems $\{111\}\langle 1\bar{1}0\rangle$ to be activated for the FCC structure.

The hardening behavior of the superalloy is recorded via the evolution of the statistically stored dislocation (SSD) density, which is accumulated with plastic strain given by

$$\rho_{SSD} = \rho_{SSD} + \gamma_{st}\dot{p}\mathrm{d}t \tag{2}$$

where γ_{st} is the hardening coefficient and $\dot{p}$ is the accumulated effective plastic strain rate. The evolution of CRSS is thus captured by

$$\tau_c^{(i)} = \tau_{c0}^{(i)} + Gb\sqrt{\rho_{SSD} + \rho_{GND}} \tag{3}$$

where $\tau_{c0}^{(i)}$ is the strain-free CRSS for slip system i, G is the shear modulus, and ρ_{GND} is the geometrically necessary dislocation density which can be computed using the Nye's dislocation tensor [21].

3. Results and Discussion

The modeling parameters can be determined for each specimen by calibrating against stress-relaxation results since the plastic strain rate was changing during the relaxation period. The determined activation energy and volume are $\Delta F = 2.50$ eV and $\Delta V = 27.56b^3$

for all four specimens. This indicates that the strain rate sensitivity does not vary with the size of γ′ precipitates, which is also evidenced by the same stress relaxation magnitude and speed in Figure 1. Similarly, since the hardening rates during the load-up periods are also similar to each other, an identical hardening coefficient $\gamma_{st} = 2500$ can be determined. On the contrary, the CRSS for specimens S1 to S4 are calculated as 30 MPa, 60 MPa, 75 MPa, and 90 MPa, respectively, which results in a classical Hall–Petch relationship [22,23]. It is worth noting that the γ′ precipitate size effect is accounted for and reflected by different CRSS values of slip systems in the CP model. In other words, the size effect is homogenized at the grain lengthscale. The strain heterogeneity can be captured with respect to grain morphology and crystal orientations, but it requires a smaller scale modeling technique (e.g., discrete dislocation plasticity) to simulate the local accumulation of plastic strain caused by precipitates.

Another important feature observed from the stress relaxation tests is that reducing the γ′ precipitate size can only enhance the strength of the superalloy, but does not contribute to the strain rate sensitivity. In other words, the gliding of dislocations is significantly affected by the γ′ precipitates, but the effects on the thermal activation events from obstacles are negligible. The strain rate sensitivity coefficient m is calculated by extracting the 0.2% offset yield stress under different strain rates according to

$$m = \mathrm{d}ln\sigma_{0.2}/\mathrm{d}ln\dot{\varepsilon} \tag{4}$$

Uniaxial tensions at constant strain rates were applied to the CP model, and the considered strain rates ranged from 1×10^{-6} s^{-1} to 1 s^{-1}, with an interval of 10 times. An identical value of $m = 0.057$ was obtained from the specimens as a result, as shown in Figure 2a).

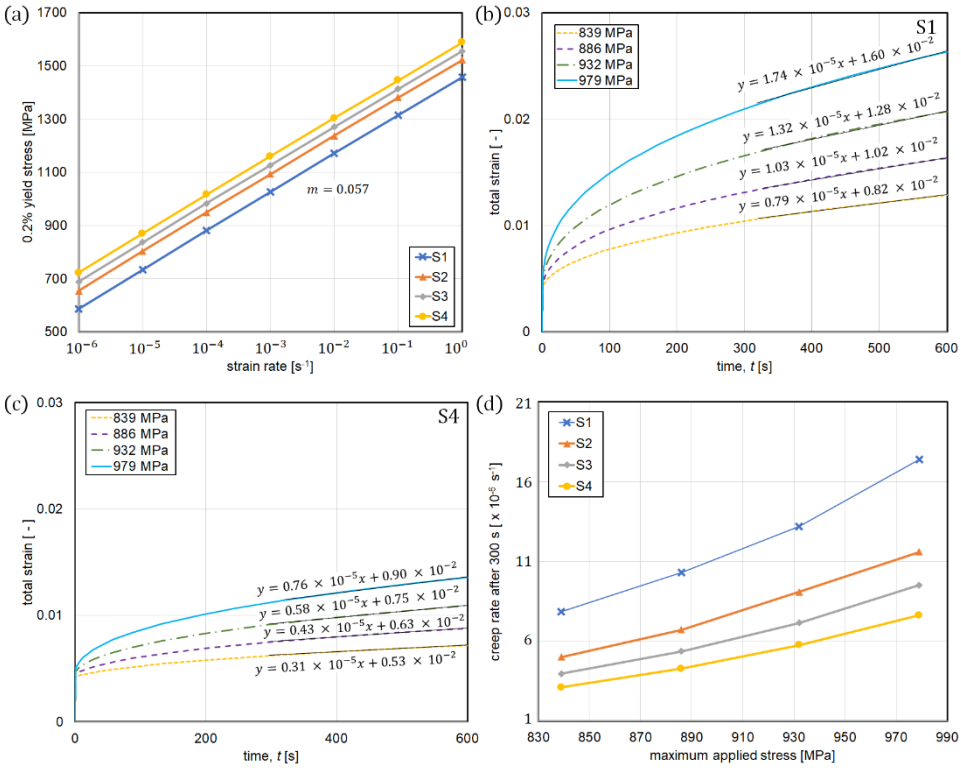


Figure 2. Strain rate sensitivity and creep responses for the superalloy. (**a**) yield stress under different strain rates; creep strain accumulations of (**b**) S1 and (**c**) S4; (**d**) creep rate after 300 s.

Although the SRS is identical for all the specimens, creep behavior may vary due to the differences in yield strength. Creep analysis was carried out using four different stress levels, i.e., 839 MPa, 886 MPa, 932 MPa, and 979 MPa, which, respectively, correspond

to 0.90, 0.95, 1.00, and 1.05 times the yield strength of specimen S1, extracted from the experimental stress-strain curve. The accumulated strain against creep time for specimens S1 and S4 are shown in Figure 2b,c. Apparent strain accumulations are observed for both specimens. The accumulation rate is higher for high-stress levels. As summarized in Figure 2d, the material with smaller γ′ precipitates shows less dependency on the stress level within the considered range due to their strong impediment for dislocation motion.

In order to validate the model, a creep strain at t = 600 s under the stress level of 932 MPa was extracted for the four specimens and compared with experimental measurements under the same conditions, as shown in Figure 3. The creep experiment was repeated three times for each microstructure to obtain reproducible results. The results display an acceptable agreement between the modeling and experiment, where the total strain generated within 600 s creep loading decreases with the reduction of the size of γ′ precipitates. Although the overall trends displayed in Figure 3 seem to corroborate this, there is still a mismatch in the strain values that need to be acknowledged, which could arise from specimen conditions that were not documented in the model, such as the inhomogeneity of dislocation and strain before applying loadings.

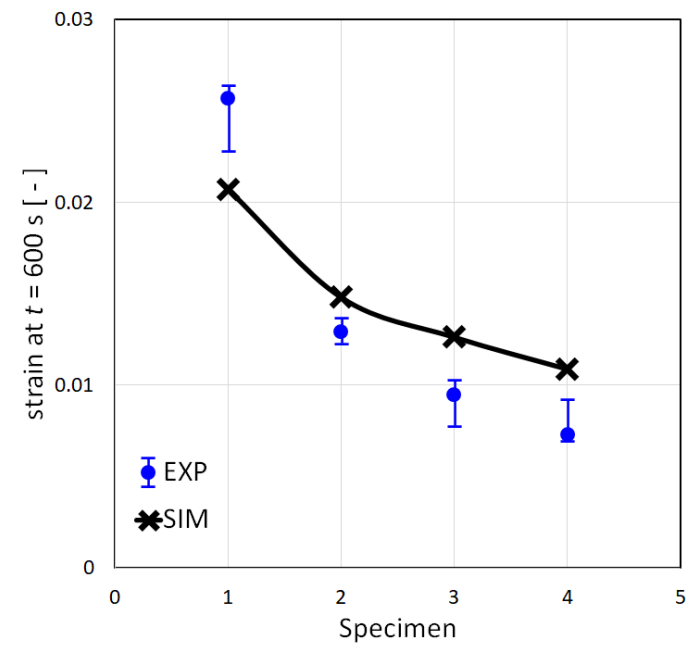


Figure 3. Creep strain at t = 600 s under the stress of 932 MPa.

The significant creep results in the differences between normal fatigue and dwell fatigue. To understand the effect of γ′ precipitates on the fatigue responses under different loading conditions, normal fatigue and dwell fatigue boundary conditions were applied to the CP model. The rise and fall time for both fatigue profiles are 1 s, while the stress-holding period is 60 s for dwell fatigue. The strain accumulation with cycles for the specimens with the largest (S1) and the smallest (S4) γ′ precipitates are compared in Figure 4. The first observation is that faster strain accumulations occur for dwell fatigue loading, exemplified by the deformation during the dwell period. Higher amounts of applied stress result in a faster strain accumulation, which is consistent with the creep results in Figure 2b–d, and leads to noticeable differences between the two fatigue types. The dwell sensitivity is also affected by the γ′ precipitates where the S4 specimen experienced lower sensitivity. It is worth noting that the influence of maximum applied stress in S4 is also smaller, especially for normal fatigue, while the total strain is almost the same.

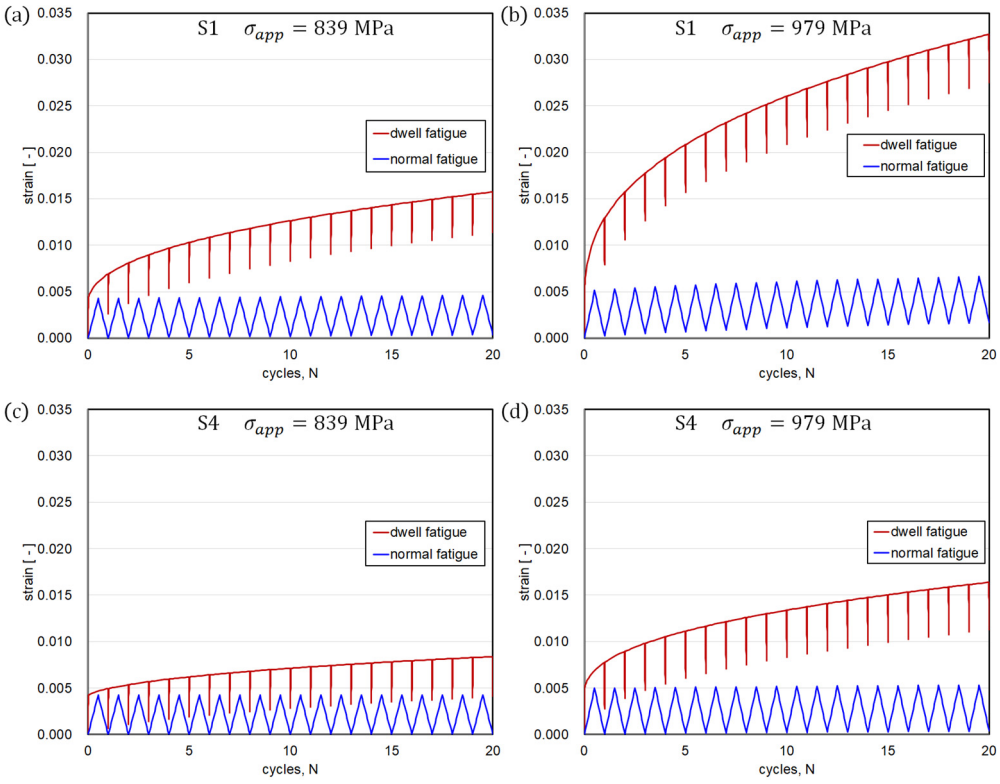


Figure 4. Strain evolutions under normal and dwell fatigue with different stress magnitudes. Specimen S1 under (**a**) 839 MPa and (**b**) 979 MPa; specimen S4 under (**c**) 839 MPa and (**d**) 979 MPa.

In addition to the macroscopic behaviors, the local stress and strain evolutions were investigated. A grain containing two columellar twins was selected, as shown in Figure 5, for detailed analysis. The crystal orientations of the parent and twin grains are schematically illustrated in the figure where the parent grain is relatively easy to deform, while the twins are hard-oriented with respect to the loading direction. The material properties in this model were chosen to represent the smallest γ′ precipitates, i.e., the S4 specimen, and the maximum applied stress is 839 MPa. The stress distribution along the loading direction under the dwell fatigue loading conditions at the onset of stress-hold of the first cycle and at the end of stress-hold of the twentieth cycle are shown in Figure 5a,b. Remarkable stress heterogeneity after 20 cycles was captured by the model. A large amount of plastic strain was generated in the parent grain under dwell fatigue, and strong slip bands were formed against the twin boundary, as indicated by the arrow in Figure 5c,d. The strain heterogeneities introduced near the twin boundaries under fatigue at 650 °C in nickel-based superalloys have been quantitatively measured experimentally by Stinville, et al. [24], using a combination of SEM and DIC techniques. They also have observed strain concentration along twin boundaries due to the development of highly localized slip bands. The strong slip bands, which developed at the boundary, redistributed stress to the twins, i.e., load shedding in parent-twin pairs. To quantitively study the load shedding, stress distributions along the path through the twin-parent boundary, before and after the first dwell period, are plotted in Figure 5e. During the first cycle, peak stress increased by ~100 MPa. With further loading cycles, the peak stress kept increasing, but the rate at which this occurred gradually reduced, as shown in Figure 5f. The local plastic strain evolution next to the twin boundary in the parent grain is also plotted in Figure 5f. Compared to the macroscopic strain accumulation under pure creep (Figure 2c), and dwell fatigue (Figure 4c), the plasticity accumulated much faster in critical regions. As a result, the local stress evolves rapidly under dwell fatigue conditions which threatens the integrity of the superalloy components.

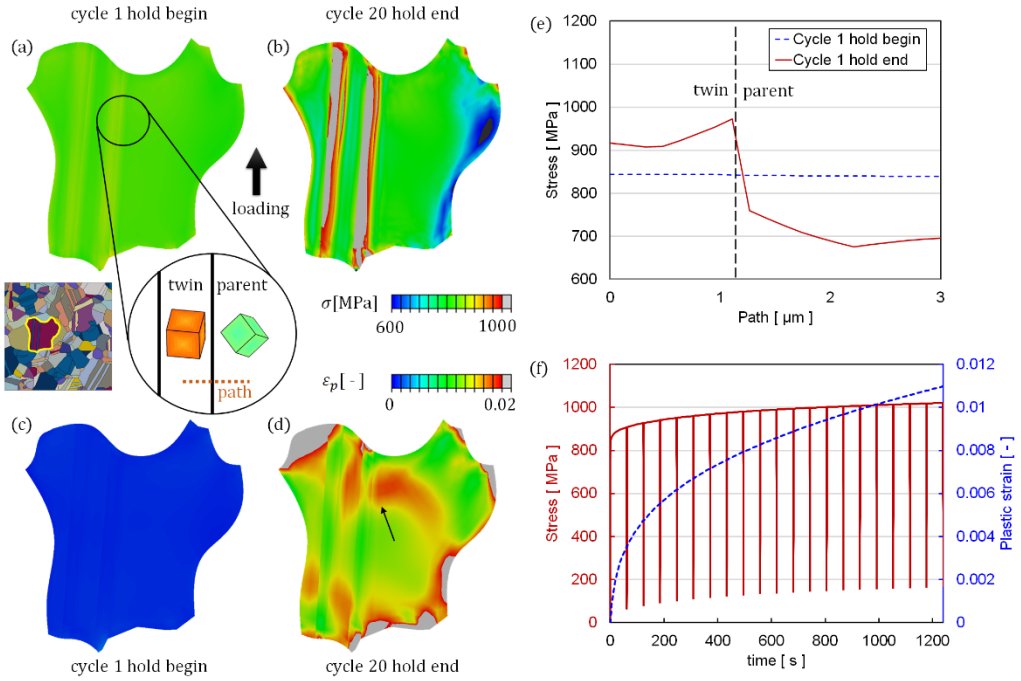


Figure 5. Microscopic stress and strain evolutions in S4 specimen under dwell fatigue loading. (**a**,**b**) Stress distributions along the loading direction. (**c**,**d**) Effective plastic strain distributions. (**e**) Load shedding along the path as sketched in (**a**). (**f**) Peak stress and plastic strain evolution with cycles.

4. Conclusions

The effect of the γ' precipitates on the rate-dependent plasticity and dwell fatigue behaviors in a PM nickel-based superalloy have been investigated using crystal plasticity finite element modeling, in which the realistic grain morphology is explicitly represented. The reduction in the size of γ' precipitates does not alter the strain rate sensitivity, but only enhances the strength of the material. Under the same loading conditions, the specimen with smaller γ' precipitates show a lower creeping rate and weaker dwell sensitivity. Load shedding between the soft parent and hard twin grains is captured by the CP model. It has been observed that the local plastic strain accumulation in the soft grain and the peak stress evolution are much faster than the macroscopic measurement.

Author Contributions: Conceptualization, Z.Z. and Z.P.; formal analysis and investigation, Z.Z. and Z.P.; writing—original draft preparation, Z.Z.; writing—review and editing, Z.P.; funding acquisition, Z.Z. and Z.P. All authors have read and agreed to the published version of the manuscript.

Funding: This research was funded by the Shenzhen Science and Technology Program, grant number: JCYJ20190806151614583, National Science Key Lab Fund, grant number: 6142903190303, and the National Natural Science Foundation of China, grant number: 91860130.

Institutional Review Board Statement: Not applicable.

Informed Consent Statement: Not applicable.

Data Availability Statement: Not applicable.

Conflicts of Interest: The authors declare no conflict of interest.

References

1. Yang, H.; Bao, R.; Zhang, J.; Peng, L.; Fei, B. Crack growth behaviour of a nickel-based powder metallurgy superalloy under elevated temperature. *Int. J. Fatigue* **2011**, *33*, 632–641. [CrossRef]
2. Jiang, J.; Yang, J.; Zhang, T.; Dunne, F.P.; Ben Britton, T. On the mechanistic basis of fatigue crack nucleation in Ni superalloy containing inclusions using high resolution electron backscatter diffraction. *Acta Mater.* **2015**, *97*, 367–379. [CrossRef]

3. Chen, B.; Jiang, J.; Dunne, F.P. Microstructurally-sensitive fatigue crack nucleation in Ni-based single and oligo crystals. *J. Mech. Phys. Solids* **2017**, *106*, 15–33. [CrossRef]
4. Peng, Z.; Zou, J.; Yang, J.; Tian, G.; Wang, X. Influence of γ' precipitate on deformation and fracture during creep in PM nickel-based superalloy. *Prog. Nat. Sci. Mater. Int.* **2021**, *31*, 303–309. [CrossRef]
5. Zhang, M.; Li, F.; Yuan, Z.; Li, J.; Wang, S. Effect of heat treatment on the micro-indentation behavior of powder metallurgy nickel based superalloy FGH. *Mater. Des.* **2013**, *49*, 705–715. [CrossRef]
6. Sinha, V.; Schwarz, R.; Mills, M.; Williams, J. Influence of hydrogen on dwell-fatigue response of near-alpha titanium alloys. *Acta Mater.* **2020**, *188*, 315–327. [CrossRef]
7. Pilchak, A.L.; Williams, J.C. Observations of Facet Formation in Near-α Titanium and Comments on the Role of Hydrogen. *Metall. Mater. Trans. A* **2010**, *42*, 1000–1027. [CrossRef]
8. Dunne, F.; Walker, A.; Rugg, D. A systematic study of hcp crystal orientation and morphology effects in polycrystal deformation and fatigue. *Proc. R. Soc. A Math. Phys. Eng. Sci.* **2007**, *463*, 1467–1489. [CrossRef]
9. Zheng, Z.; Balint, D.S.; Dunne, F.P. Discrete dislocation and crystal plasticity analyses of load shedding in polycrystalline titanium alloys. *Int. J. Plast.* **2016**, *87*, 15–31. [CrossRef]
10. Hasija, V.; Ghosh, S.; Mills, M.J.; Joseph, D.S. Deformation and creep modeling in polycrystalline Ti–6Al alloys. *Acta Mater.* **2003**, *51*, 4533–4549. [CrossRef]
11. Sinha, V.; Mills, M.J.; Williams, J.C.; Spowart, J.E. Observations on the faceted initiation site in the dwell-fatigue tested ti-6242 alloy: Crystallographic orientation and size effects. *Metall. Mater. Trans. A* **2006**, *37*, 1507–1518. [CrossRef]
12. Zhang, Z.; Dunne, F.P. Microstructural heterogeneity in rate-dependent plasticity of multiphase titanium alloys. *J. Mech. Phys. Solids* **2017**, *103*, 199–220. [CrossRef]
13. Kumar, S.S.; Raghu, T.; Bhattacharjee, P.; Rao, G.A.; Borah, U. Strain rate dependent microstructural evolution during hot deformation of a hot isostatically processed nickel base superalloy. *J. Alloys Compd.* **2016**, *681*, 28–42. [CrossRef]
14. Lu, H.; Jia, X.; Zhang, K.; Yao, C. Fine-grained pretreatment process and superplasticity for INCONEL718 superalloy. *Mater. Sci. Eng. A* **2002**, *326*, 382–385. [CrossRef]
15. Peng, Z.; Tian, G.; Jiang, J.; Li, M.; Chen, Y.; Zou, J.; Dunne, F.P. Mechanistic behaviour and modelling of creep in powder metallurgy FGH96 nickel superalloy. *Mater. Sci. Eng. A* **2016**, *676*, 441–449. [CrossRef]
16. Stinville, J.; Lenthe, W.; Miao, J.; Pollock, T. A combined grain scale elastic–plastic criterion for identification of fatigue crack initiation sites in a twin containing polycrystalline nickel-base superalloy. *Acta Mater.* **2016**, *103*, 461–473. [CrossRef]
17. Stinville, J.; Vanderesse, N.; Bridier, F.; Bocher, P.; Pollock, T. High resolution mapping of strain localization near twin boundaries in a nickel-based superalloy. *Acta Mater.* **2015**, *98*, 29–42. [CrossRef]
18. Latypov, M.I.; Stinville, J.-C.; Mayeur, J.R.; Hestroffer, J.M.; Pollock, T.M.; Beyerlein, I.J. Insight into microstructure-sensitive elastic strain concentrations from integrated computational modeling and digital image correlation. *Scr. Mater.* **2021**, *192*, 78–82. [CrossRef]
19. Zhang, X.; Stinville, J.-C.; Pollock, T.M.; Dunne, F.P. Crystallography and elastic anisotropy in fatigue crack nucleation at nickel alloy twin boundaries. *J. Mech. Phys. Solids* **2021**, *155*, 104538. [CrossRef]
20. Dunne, F.; Rugg, D.; Walker, A. Lengthscale-dependent, elastically anisotropic, physically-based hcp crystal plasticity: Application to cold-dwell fatigue in Ti alloys. *Int. J. Plast.* **2007**, *23*, 1061–1083. [CrossRef]
21. Dunne, F.P.E.; Kiwanuka, R.; Wilkinson, A.J. Crystal plasticity analysis of micro-deformation, lattice rotation and geometrically necessary dislocation density. *Proc. R. Soc. A Math. Phys. Eng. Sci.* **2012**, *468*, 2509–2531. [CrossRef]
22. Hall, E.O. The Deformation and Ageing of Mild Steel: III Discussion of Results. *Proc. Phys. Soc. Sect. B* **1951**, *64*, 747–753. [CrossRef]
23. Petch, J.N. The Cleavage Strength of Polycrystals. *J. Iron Steel Inst.* **1953**, *174*, 25–28.
24. Stinville, J.-C.; Echlin, M.P.; Callahan, P.G.; Miller, V.M.; Texier, D.; Bridier, F.; Bocher, P.; Pollock, T.M. Measurement of Strain Localization Resulting from Monotonic and Cyclic Loading at 650 °C in Nickel Base Superalloys. *Exp. Mech.* **2017**, *57*, 1289–1309. [CrossRef]